Original paper

Magnesian tourmalines from plagioclase–muscovite–scapolite metaevaporite layers in dolomite marble near Prosetín (Olešnice Unit, Moravicum, Czech Republic)

Peter BAČÍK[1,*], Pavel UHER[1], Jan CEMPÍREK[2,3], Tomáš VACULOVIČ[4]

[1] *Comenius University in Bratislava, Faculty of Natural Sciences, Department of Mineralogy and Petrology, Mlynská dolina, 842 15 Bratislava, Slovak Republic; bacikp@fns.uniba.sk*
[2] *Department of Mineralogy and Petrography, Moravian Museum, Zelný trh 6, 659 37 Brno, Czech Republic*
[3] *Department of Earth and Ocean Sciences, University of British Columbia, 6339 Stores Road, Vancouver, BC, V6T 164 Canada*
[4] *Central European Institute of Technology, Masaryk University, Kamenice 5, 625 00 Brno, Czech Republic*
[*] *Corresponding author*

Radial aggregates of blue–grey tourmaline were found in plagioclase–muscovite–scapolite metaevaporite layers in dolomite marble near Prosetín (Olešnice Unit, Moravicum, Czech Republic). It occurs in association with plagioclase ($An_{15–37}$), muscovite, scapolite, phlogopite, vermiculite, pumpellyite-(Al), and clinozoisite. Electron-microprobe analyses of tourmaline show dravitic composition with very high content of Mg (1.92 to 2.77 *apfu*), Al (up to 6.71 *apfu*), low content of Fe (up to 0.39 *apfu*) and variable amounts of vacancies (0.09 to 0.47) and Ca (0.03 to 0.29 *apfu*) in the *X*-site. Some analyses correspond to "oxy-dravite" and some others almost attain magnesio-foitite compositions. The proportion of *X*-site vacancy decreases from the crystal cores to their rims while Ca content increases. Generally, charge excess due to the high Al-contents is balanced either by an increasing *X*-site vacancy or by deprotonization of ^WOH; the $^WO^{2–}$ content calculated from charge-balanced formula attains 0.71 *apfu*. Lattice parameters [a = 15.9116(6) Å; c = 7.1987(4) Å] and deduced average bond lengths (<*Y*-O> = 1.995 Å; <*Z*-O> = 1.929 Å) indicate a relatively high Al–Mg disorder. Three main substitution mechanisms are inferred to operate in the studied magnesian tourmalines: (1) $CaMg(NaAl)_{-1}$, mainly in Ca-enriched dravite, (2) $^X\square Al(NaMg)_{-1}$ in nearly magnesio-foititic compositions, and (3) $AlO(MgOH)_{-1}$ in "oxy-dravitic" members. The tourmaline is relatively poor in trace elements; only Ti, Sr, and Ga exceed 100 ppm according to LA-ICP-MS study. There is a pronounced positive correlation between Sr and Ca (r^2 = 0.77), which suggests that Sr accumulated in Ca-enriched zones of dravite. The pale blue–grey color of the studied tourmalines is most likely a result of Fe^{2+} crystal field transitions along with the absence of significant amounts of other chromophores. Trace-element contents, mineral assemblage and compositional zoning of tourmalines as well as host-rock mineral association suggest prograde metamorphic growth and support metaevaporitic origin of the plagioclase–muscovite–scapolite rocks.

Keywords: tourmaline, dravite, oxy-dravite, crystal chemistry, metaevaporites, Bohemian Massif
Received: 17 May 2012; accepted: 14 September 2012; handling editor: M. Novák

1. Introduction

Extremely magnesian tourmaline including dravite, "oxy-dravite" and magnesio-foitite is confined to specific genetic environment. It requires high atomic X_{Mg} [Mg/(Mg + Fe)] ratio in the host rock, and thus is characteristic of metaultramafic rocks, metapyroxenites, or metacarbonates (Henry and Guidotti 1985). Another typical host for highly magnesian tourmalines are metaevaporites, where oxy-dravite and dravite frequently occur (Henry et al. 1999, 2008; Žáček et al. 2000; Bačík et al. 2008). This compositional feature of tourmaline is attributed to the influence of oxidizing, highly saline, boron-bearing fluids associated with such lithologies (Henry et al. 2008). Formation of tourmaline is a result of subsequent metamorphic events, whereby the high X_{Mg} ratio is determined by the bulk composition of the host Mg-rich marine evaporite.

Plagioclase–muscovite–scapolite rock layers in dolomite marble near Prosetín (Olešnice Unit, Moravicum, Czech Republic) host tourmaline which belongs to dravite–oxy-dravite and dravite–magnesio-foitite solid solutions. Although it has been studied previously by powder X-ray diffraction (XRD), wet chemical analysis (Povondra and Novák 1986) and also electron microprobe analysis (EMPA) (Opletal 2009), we bring new detailed mineralogical and crystallochemical data resulting from application of EMPA, powder XRD, and Laser Ablation Inductively Coupled Plasma Mass Spectrometry (LA-ICP-MS). These provide new insights on the tourmaline composition, structural properties, origin, and on the chromophores responsible for its blue–grey color.

2. Geological setting

The studied locality belongs to Olešnice Unit, Moravicum, which is a part of the Moravo–Silesian Zone in the eastern Bohemian Massif. The Moravo–Silesian Zone represents a Hercynian nappe complex which is structurally underlying the Moldanubian metamorphic complex (Neubauer and Handler 2000; Finger et al. 2007; Schulmann et al. 2008). The Moravo–Silesian Zone represents a NE–SW trending belt of Neoproterozoic to Lower Paleozoic sheared and metamorphosed rocks derived from the Brunia microcontinent (Kalvoda et al. 2008). This ~300 km long, 30 to 50 km wide belt consists of three NE–SW-elongated tectonic windows emerging through structurally overlying high-grade rocks of the Moldanubian–Lugian domain: southern Thaya Window; central Svratka Window and northern Silesian domain (Schulmann et al. 2008). The Moravo–Silesian Zone developed during Carboniferous dextral-oblique thrusting of the Moldanubian–Lugian domain (Schulmann et al. 1991).

The lithotectonic structure of the Svratka Window (including the Olešnice Unit) is, from bottom to top and from the East to the West, as follows: (1) The Parautochthonous domain (chlorite zone), (2) Lower Moravian Nappe (biotite zone), and (3) Upper Moravian Nappe (garnet zone). Consequently, the Svratka Window is characterized by inverted Barrovian metamorphic zonation (Ulrich et al. 2002). The Olešnice Unit (Olešnice–Vranov Unit) represents a variegated lithologic sequence of predominantly Devonian (?) metamorphic rocks, mainly mica schists and paragneisses, graphitic metapelites, quartzites, calcite and dolomite marbles, rarely amphibolites and metagabbros (Sekanina 1965a; Opletal et al. 2007). The tremolite-bearing marbles of the Olešnice Unit build the upper parts of the Upper Moravian Nappe, where they form large bodies (up to 50 m thick) set in a complex of dominant muscovite–biotite metapelites (mica schists and gneisses) metamorphosed in amphibolite facies (garnet zone). The P–T–X conditions of metamorphism of these marbles were estimated from stability of the assemblages tremolite + calcite + quartz and tremolite + dolomite, corresponding to $T_{max.} = 580–620\,°C$ at $X(CO_2) = 0.2–0.7$ and $T_{min.} = 480–530\,°C$ at $X(CO_2) = 0.2–0.6$ at $P_{total} = 500$ MPa (Houzar et al. 2000; Houzar and Leichmann 2003).

At the disused Prosetín quarry, the studied locality (49.534933° N, 16.398883° E, 613 m above sea level), two parallel layers of concordant muscovite–plagioclase–scapolite rock are enclosed in dolomite marble; the layers are usually c. 30 cm, locally up to 50 cm thick. Elsewhere, their thickness reaches only 10 cm or they wedge out completely (Opletal et al. 2007; Opletal 2009).

There are two hypotheses regarding the origin of plagioclase–muscovite rock layers in dolomite marble near Prosetín. Sekanina (1965b) considered the plagioclase–muscovite rock layers to be intrusions of SiO_2-poor aplites (oligoclasites) and explained the scapolite- and tourmaline-bearing mineral association as a result of interaction of hydrothermal fluids with oligoclasite. In contrast, Opletal et al. (2007) showed that plagioclase–muscovite–scapolite rock layers may be of metaevaporitic origin. The latter hypothesis is supported e.g. by the absence of Mg skarns with diopside and/or forsterite zones, which are otherwise a typical product of the interaction between granitic–pegmatitic magma and dolomites (e.g., Shabynin 1973), absence of lateral veins characteristic of pegmatites and inferred high activity of Cl required for crystallization of the Cl-enriched marialite ($Mar_{51–59}$) present in the assemblage (Opletal et al. 2007). Two metamorphic phases in the plagioclase–muscovite–scapolite rocks – (1) prograde, producing association of scapolite, phlogopite, part of clinozoisite and plagioclase with $An_{15–37}$, and (2) retrograde, with albite, chlorite, muscovite and vermiculite – generally correlate with evolution of the surrounding dolomite marble. Plagioclase associated with tourmaline is altered to muscovite, albite, epidote and calcite; the tourmaline assemblage was formed likely at the end of the prograde or at the beginning of the retrograde phase (Opletal et al 2007; Opletal 2009).

3. Analytical methods

The composition of tourmaline was established with CAMECA SX100 electron microprobe in wavelength-dispersion mode, at the State Geological Institute of Dionýz Štúr, Bratislava. The analytical conditions were: accelerating voltage 15 kV, beam current 20 nA, and beam diameter of 3 to 5 μm. The tourmaline samples were analyzed with the following standards: wollastonite (SiK_α, CaK_α), TiO_2 (TiK_α), Al_2O_3 (AlK_α), pure Cr (CrK_α), pure V (VK_α), fayalite (FeK_α), rhodonite (MnK_α), forsterite (MgK_α), willemite (ZnK_α), pure Ni (NiK_α), albite (NaK_α), orthoclase (KK_α), BaF_2 (FK_α) and NaCl (ClK_α). Lower detection limits of the measured elements varied between 0.01 and 0.05 wt. %; V, Cr, Mn, Zn, Ni, F, and Cl were also below their respective detection limits. The analytical data were normalized according to the PAP procedure (Pouchou and Pichoir 1985). The crystallochemical formulae of tourmaline were calculated on the basis of 15 $Y + Z + T$ cations, $^{W}O^{2–}$ was obtained from the charge-balanced formula, OH was calculated as OH $= 4 – Cl – {}^{W}O$ apfu, B = 3 apfu.

Powder X-ray diffraction analyses were made on diffractometer BRUKER D8 Advance (Laboratory of

X-ray diffraction SOLIPHA, Faculty of Natural Sciences, Comenius University in Bratislava) under following conditions: Bragg–Brentano geometry (Theta–2 Theta), Cu anticathode (λ_α = 1.54060 Å), accelerating voltage 40 kV, beam current 40 mA. Ni K_β filters were used for stripping of K_β radiation on the primary and diffracted beam, and data were acquired by the BRUKER Lynx-Eye detector. The step size was 0.01° 2Θ, the step time 5 s per step, and the range of measurement 4 to 65° 2Θ. Measured data were evaluated with the DIFFRAC[plus] EVA software package. Analyzed scans were fitted by, and lattice parameters refined with, the DIFFRAC[plus] TOPAS software on a basis of dravite structure (sample 32008, Bloodaxe et al. 1999). Average bond lengths in octahedra were calculated from lattice parameters according to empirical formulae: a = 13.045 + 1.437 <*Y*-O> Å; c = 0.886 + 3.272 <*Z*-O> Å (Bosi and Lucchesi 2004). Subsequently, it allowed to calculate ^{Z}Mg in crystallochemical formulae according to empirical formula ^{Z}Mg = 49.697<*Z*-O> – 94.845 (Ertl et al. 2010).

The LA-ICP-MS analyses were carried out by a laser ablation system UP 213 (New Wave, USA) attached to a quadrupole ICP-MS Agilent 7500 CE (Agilent, Japan), at the Central European Institute of Technology, Masaryk University, Brno. The Q-switched Nd-YAG laser emits radiation with wavelength of 213 nm. The sample gas flow of Ar (0.6 l/min) was admixed to the He carrier gas (1.0 l/min) behind the laser ablation cell. The LA-ICP-MS parameters were optimized using the glass reference material NIST SRM 612 to yield a maximum signal to noise ratio. Hole drilling mode of laser ablation was utilized with spot diameter 65 μm, laser beam fluency 18 J.cm^{-2} and repetition rate 10 Hz, ablating for 40 s at each spot. All element contents were normalized using Si as an internal standard; its content was obtained by EMPA.

4. Results

Tourmaline from Prosetín forms radial aggregates of blue–grey prismatic crystals, up to 3 cm across (Fig. 1). It has very weak chemical zoning; three compositional types of tourmaline were recognized, occurring in variable proportions. Two zones can be distinguished in BSE: light one, generally forming cores of crystals (if they are defined by surfaces of prisms), and dark one, on the rim (Fig. 2). The light zone consists of two phases with different chemical compositions: (1) tourmaline with higher *X*-site vacancy and compositions changing from dravite toward magnesio-foitite, and (2) tourmaline with low *X*-site vacancy and Ca concentrations which attains the oxy-dravite composition (Tab. 1, Figs 2 to 4). The dark zone at the rim (Fig. 2 – phase no. 3) is formed by dravite

with increased Ca (Tab. 1, Figs 2 to 4). The enrichment in Ca is likely the result of the uvite substitution mechanism, CaMg(NaAl)$_{-1}$ (Fig. 5a).

All zones of the Prosetín tourmaline are strongly magnesian (X_{Mg} = 0.85–0.92, and up to 0.97 in Ca-enriched dravite; Tab. 1). The studied tourmaline has an increased content of Al relative to the ideal composition of dravite. In dravite to magnesio-foitite, it varies between 6.42 and 6.48 *apfu*, and between 6.28 and 6.72 *apfu* in oxy-dravitic zones. The lowest content of Al is in Ca-enriched compositions, but still reaches up to 6.25 *apfu* Al (Fig. 4, Tab. 1). The increased Al contents may be charge-balanced by the increase in *X*-site vacancy due to the ^{X}□Al(NaMg)$_{-1}$ substitution (Fig. 5b). However, this mechanism may be significant only in the dravite–magnesio-foitite phase, as the proportion of *X*-site vacancy in oxy-dravite is too
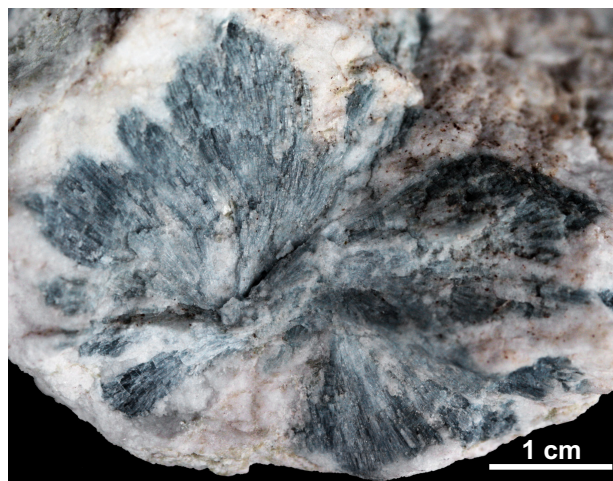
Fig. 1 Radial aggregate of tourmaline crystals from Prosetín.
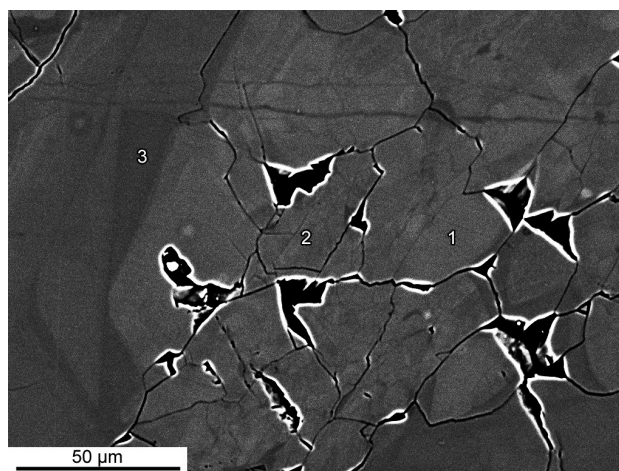
Fig. 2 Back-scattered electron (BSE) image of zoned tourmaline from Prosetín. 1 – zone enriched in *X*-site vacancy; 2 – zone with low *X*-site vacancy and Ca contents – „oxydravite"; 3 – zone enriched in Ca.

Tab. 1 Representative electron-microprobe analyses of tourmaline from Prosetín (in wt. % and *apfu*)

	Phase 1	Phase 1	Phase 2	Phase 2	Phase 3	Phase 3
SiO_2	38.42	38.24	37.80	37.32	37.54	37.67
TiO_2	b.d.l.	b.d.l.	b.d.l.	0.03	0.03	0.04
B_2O_3*	10.89	10.81	10.85	10.72	10.81	10.84
Al_2O_3	34.33	33.81	35.56	33.99	32.79	32.90
FeO	2.48	2.36	2.11	2.00	0.60	0.52
MgO	8.71	8.83	8.10	9.03	11.13	11.14
CaO	0.13	0.17	0.39	0.98	1.66	1.62
Na_2O	1.62	1.61	2.34	2.18	1.84	1.72
K_2O	0.03	0.00	0.03	0.03	0.03	0.02
H_2O*	3.49	3.47	3.08	3.12	3.32	3.37
Total	100.15	99.35	100.33	99.40	99.76	99.93
Si	6.132	6.151	6.057	6.049	6.034	6.038
B	3.000	3.000	3.000	3.000	3.000	3.000
Al	4.962	4.964	4.958	4.964	4.963	4.963
Mg	1.036	1.036	1.036	1.036	1.036	1.036
$\sum Z$	6.000	6.000	6.000	6.000	6.000	6.000
Ti	–	–	–	0.003	0.004	0.005
Al	1.497	1.446	1.758	1.530	1.249	1.252
Fe	0.332	0.317	0.283	0.271	0.081	0.070
Mg	1.037	1.082	0.900	1.146	1.632	1.626
$\sum Y$	2.868	2.849	2.943	2.951	2.966	2.962
Ca	0.022	0.030	0.067	0.170	0.286	0.278
Na	0.502	0.502	0.728	0.686	0.573	0.536
K	0.005	0.002	0.005	0.006	0.005	0.005
$^X\square$	0.471	0.466	0.200	0.139	0.135	0.182
O	0.277	0.275	0.703	0.628	0.441	0.397
OH	3.720	3.725	3.295	3.370	3.559	3.603
$\sum V+W$	4.000	4.000	4.000	4.000	4.000	4.000
$\sum$cations	18.529	18.534	18.800	18.861	18.865	18.818
$\sum$Al	6.459	6.410	6.717	6.494	6.212	6.216

* contents calculated from ideal stoichiometry

b.d.l. = below detection limit; Phases – see Fig. 2

Tab. 2 Powder X-ray diffraction pattern of Prosetín tourmaline

h	k	l	$d_{obs.}$ (Å)	I (%)	$d_{calc.}$ (Å)
1	1	0	7.92	5	7.96
1	0	1	6.36	22	6.38
0	2	1	4.967	13	4.979
3	0	0	4.582	23	4.595
2	1	1	4.210	34	4.221
2	2	0	3.970	100	3.979
0	1	2	3.474	38	3.483
1	3	1	3.370	10	3.377
4	0	1	3.103	6	3.108
4	1	0	3.003	20	3.008
1	2	2	2.956	36	2.962
3	2	1	2.889	7	2.895
3	1	2	2.618	6	2.621
0	5	1	2.571	41	2.575
0	0	3	2.3946	9	2.3999
2	3	2	2.3728	7	2.3758
5	1	1	2.3378	10	2.3412
5	0	2	2.1853	5	2.1887
4	3	1	2.1586	7	2.1616
0	3	3	2.1240	6	2.1272
4	2	2	2.1071	5	2.1104
2	2	3	2.0519	7	2.0551
1	5	2	2.0370	13	2.0399
1	6	1	2.0147	5	2.0178
4	4	0	1.9864	4	1.9896
3	4	2	1.9157	10	1.9178
1	4	3	1.8736	4	1.8760
6	2	1	1.8448	4	1.8475
3	3	3	1.7770	3	1.7797
0	6	3	1.6574	5	1.6596
2	7	1	1.6378	5	1.6397
4	0	4	1.5943	3	1.5954
5	5	0	1.5902	8	1.5917
4	5	2	1.5833	2	1.5847
4	6	1	1.5428	3	1.5443

Tab. 3 Lattice parameters and bond lengths of octahedral sites comparing tourmaline from Prosetín with published data

Locality	Reference	Mineral	*a* [Å]	*c* [Å]	*V* [Å³]	<*Y*-O>* [Å]	<*Z*-O>* [Å]	^{Z}Mg[†] (*apfu*)	Method
Prosetín, Czech Republic	this work	dravite to oxy-dravite	15.9116(6)	7.1987(4)	1578.37(8)	1.995	1.929	1.036	PXRD
Prosetín, Czech Republic	Povondra and Novák (1986)	dravite	15.908(3)	7.192(3)	1576.1(7)	1.992	1.927	0.934	PXRD
Gemerská Poloma, Slovakia	Bačík et al. (2011a)	dravite	15.9289(7)	7.2132(17)	1584.99(15)	2.007	1.934	1.256	PXRD
Forshammar, Sweden	Bačík et al. (in print)	dravite	15.9223(6)	7.1706(5)	1574.34	2.002	1.921	0.7	SREF
Bajkal, Russia[1]	Bosi and Lucchesi (2004)	oxy-dravite	15.9030(7)	7.1951(4)	1575.89	2.011	1.930	0.991	SREF
Small Falls, USA[2]	Bloodaxe et al. (1999)	oxy-dravite	15.945(1)	7.169(1)	1578.58	2.018	1.920	0.635	SREF
Steinthaller, Austria[3]	Ertl et al. (2010)	fluor-dravite	15.9354(4)	7.1934(4)	1581.94	2.011	1.928	0.75	SREF
Kyonosawa, Japan	Hawthorne et al. (1999)	magnesio-foitite	15.884(4)	7.178(3)	1568.0(6)	1.976	1.923	–	SREF

[1]sample 9840f; [2] sample Ru-T18-92; [3]sample STE; lattice parameters from PXRD – powder XRD, SREF – structure refinement;

* – bond lengths calculated according to empirical formulae by Bosi and Lucchesi (2004); [†] ^{Z}Mg obtained by the empirical formula of Ertl et al. (2010).
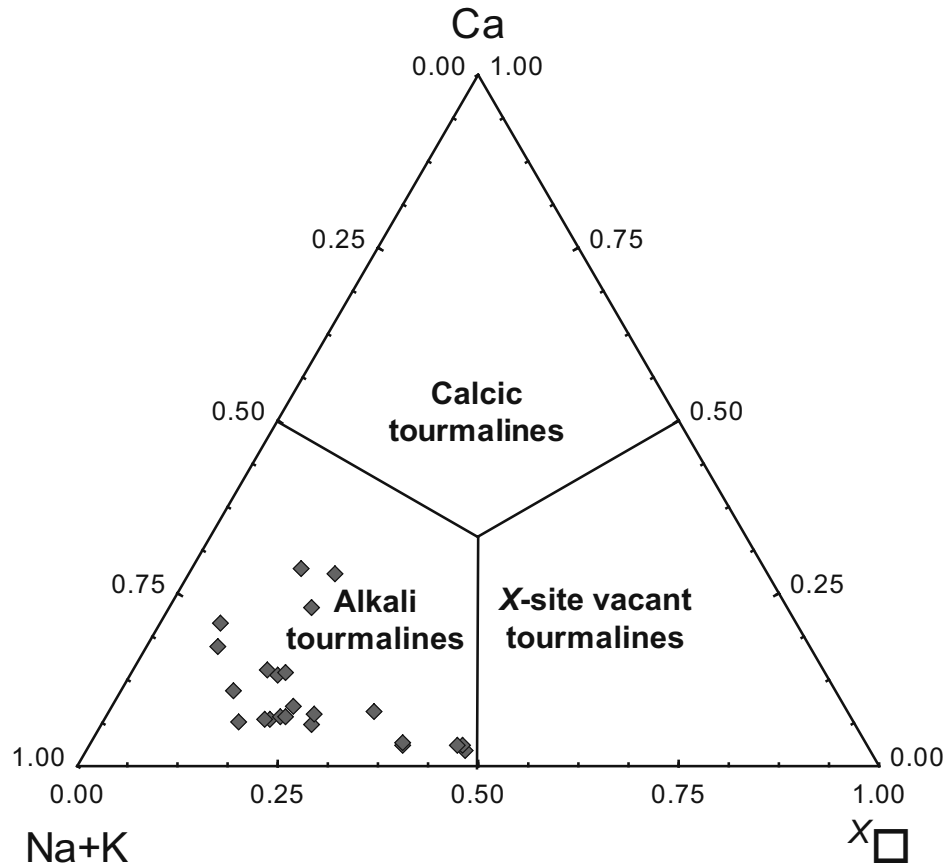
Fig. 3 – Classification diagram (Na + K)–Ca–$^X\square$ for minerals of tourmaline supergroup.

low to balance charge excess sufficiently. In contrast, the increase in the Al correlates with the ^WO contents calculated from the charge-balanced formula (Tab. 1). This suggests a strong influence of the $AlO(MgOH)_{-1}$ substitution.

Powder XRD data (Tables 2 and 3) are strongly influenced by the compositional variations of the studied tourmaline. However, based on BSE observations and EMPA study, oxy-dravite and magnesio-foitite phases are dominant and they differ only slightly in Al and Mg contents (Tab. 1). Average bond lengths in octahedral sites calculated from lattice parameters were compared to published data; the mean $<Y\text{-}O>$ bond length in the studied tourmaline is shorter than those published for dravite, "oxy-dravite" and fluor-dravite, but longer than in magnesio-foitite (Tab. 3). This corresponds well with the higher contents of Al in the Y site. In contrast, the $<Z\text{-}O>$ bond is relatively long, which could suggest a significant proportion of Mg^{2+} with higher ionic radius than Al^{3+} in the octahedral coordination (0.72 and 0.535 Å, respectively; Shannon 1976).

Tourmaline from Prosetín is relatively poor in trace elements. Only Ti, Sr, and Ga attain more than 100 ppm, the contents of Sc, Mn, Ni, Zn and Sn vary between 10 and 100 ppm (Tab. 4). The REE contents are even lower; only La, Ce, Nd and Y exceed their respective

detection limits. There is an apparent correlation of Ti and Sr with Ca (Fig. 6), which suggests that the former two elements are accumulated in Ca-enriched zones of dravite.

Tab. 4 Contents of trace elements (ppm) in Prosetín tourmaline – analyzed by LA-ICP-MS

in ppm	Minimum	Maximum	Limit of detection
Ca	2400	10500	1700
Sc	13	36	11
Ti	24	470	13
V	<1	7	1
Mn	22	60	8
Co	2	7	0.9
Ni	5	23	5
Zn	17	45	4
Ga	73	122	0.5
Sr	95	337	1
Y	<0.01	3	0.01
Sn	9	22	6
La	<0.1	2	0.1
Ce	1	4	0.1
Nd	<0.01	4	<0.01
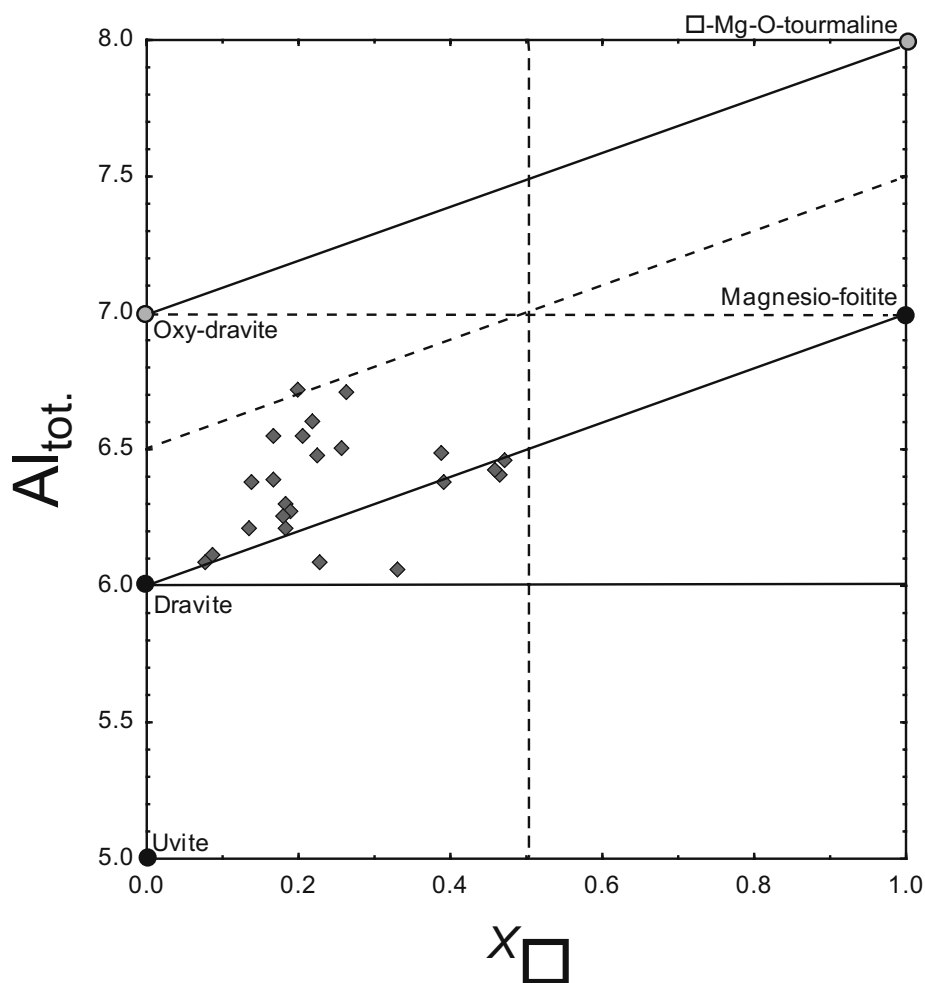
Fig. 4 – Diagram Al vs. $^X\square$ with end-members of the tourmaline supergroup and substitution trends.

5. Discussion and conclusions

5.1 Crystal chemistry of tourmaline

Calculation of bond lengths in octahedral sites on a basis of empirical formulae from lattice parameters is appropriate method if no structure-refinement data are available. Besides giving partial information on the structure geometry, it also helps to solve problems with site occupancy and crystal chemistry of mineral. Site occupancy and cation distribution has many effects not only on the geometry of Y and Z octahedra but on the entire structure of tourmaline. Octahedral dimensions influence lattice parameters; the parameter a correlates with $<Y-O>$ bond length, whereas c is correlated with the $<Z-O>$ bond length (Bosi and Lucchesi 2004). The $<Z-O>$ bond length in octahedra entirely occupied by Al, as in elbaite, rossmanite, olenite and foitite, varies between 1.90 and 1.91 Å (e.g., Grice and Ercit 1993; MacDonald et al. 1993; Burns et al. 1994; Selway et al. 1998, Cempírek et al. 2006). In contrast, the $<Z-O>$ bond length in Mg-bearing tourmalines is in the range of 1.92 to 1.93 Å (e.g., Bloodaxe et al. 1999; Hawthorne

et al. 1999; Bosi and Lucchesi 2004; Ertl et al. 2010; Bačík et al. 2011a, in print). There is a good correlation between ^{Z}Mg content and the $<Z-O>$ bond length (Ertl et al. 2010): the $<Z-O>$ bond length increases with the ^{Z}Mg (or other cations with ionic radius larger than Al, if present). Significant amounts of Mg may enter the Z site due to Al–Mg disorder even if the Al content exceeds 6 *apfu* and could be sufficient to fill the Z site entirely (e.g., Grice and Ercit 1993; Hawthorne et al. 1993, 1999; Bloodaxe et al. 1999; Bosi and Lucchesi 2004; Ertl et al. 2010). The studied tourmalines have affinity to magnesio-foitite and oxy-dravite with a relatively high value of the $<Z-O>$ bond length (1.929 Å), despite of their Al-rich composition (up to 6.72 Al *apfu*). Therefore, the total amount of Al is not a key factor determining the Z-site occupancy in Mg-bearing tourmalines. The disorder of Al and Mg among the octahedral sites is controlled by different mechanisms, due to short-range bond-valence requirements (e.g. Hawthorne 2002); in any case, it is reflected by the W-site occupancy. If the W site is fully occupied by OH, only 3^YR^{2+} or $2^YR^{2+}+^YR^{3+}$ cation structural arrangements are stable, in contrast to the 3^YR^{3+} or $2^YR^{3+}+^YR^{2+}$

cation arrangements which are found in $^W\!O^{2-}$-dominant "oxy-tourmalines" (Hawthorne 2002). Calculated $^W\!O$ proportion therefore suggests relatively large degree of Al–Mg disorder in the studied samples, at least in the oxy-dravite compositions. Significant role of de-protonized O in the *W* site of the Prosetín tourmaline was also confirmed by wet chemical analysis ($^{(V+W)}\!OH$ = 3.68 *pfu*) of Povondra and Novák (1986). On the other hand, since the disorder is commonly present in (OH,F)-dominant tourmalines, the disorder-controlling factor must be the thermodynamic stability of the *Y, Z* site configuration within the specific tourmaline composition. Good examples include the magnesio-foitite from Kyonosawa, Japan (Hawthorne et al. 1999), and fluor-dravite from Steinthaller, Austria (Ertl et al. 2010) which lack $^W\!O$ but they seem to be medium to strongly disordered. Possible factors for *Y* site contents and Al–Mg disorder discussed in the literature include *X* site contents (e.g. Ertl et al. 2010), Fe/(Fe + Mg) ratio (Grice and Ercit 1993), structure deformations (Foit 1989; Bosi and Lucchesi 2007) or temperature (Ertl et al. 2008; Bosi 2011). Besides a minor Ca-content (uvite component), the high amount of *X*-site vacancies plays a significant role in $^W\!O$-poor dravite–magnesio-foitite phase of the Prosetín tourmaline.

The size of *Y* octahedron depends on the synergic effect of the various cations occupying the site. This is a net result of an interplay between the size contraction owing to the presence of smaller cations ($^Y\!Al^{3+}$, $^Y\!Li^+$) and size-expansion caused by $^Y\!Fe^{2+}$, $^Y\!Mg^{2+}$, and $^Y\!V^{3+}$ with larger ionic radii (Bosi and Lucchesi 2004). The <*Y*-O> bond length may decrease to 1.96 Å in olenite with *Y* site dominated by Al (Hughes et al. 2000), 2.00 Å in elbaite with *Y* site occupied by Al and Li (Burns et al. 1994; Bosi et al. 2005), and 1.98 Å in magnesio-foitite with $^Y\!Mg$ and $^Y\!Al$ (Hawthorne et al. 1999). On the other hand, this parameter increases to 2.05 Å in $^Y\!Fe^{2+}$-dominant schorl (Grice and Ercit 1993; Bloodaxe et al. 1999; Bosi and Lucchesi 2004). The typical value of the <*Y*-O> bond length in $^Y\!Mg$-dominant dravitic–"oxy-dravitic" tourmalines varies between 2.00 and 2.01 Å (Bloodaxe et al. 1999; Bosi and Lucchesi 2004; Ertl et al. 2010; Bačík et al. 2011a, in print). Thus, lower value of the <*Y*-O> bond length in Prosetín relative to other dravitic tourmalines is obviously the cumulative effect of very low Fe²⁺ and relatively high $^Y\!Al$ contents owing to: (1) AlO(MgOH)$_{-1}$ substitution mostly in the "oxy-dravite" phase; (2) $^X\!\square Al(NaMg)_{-1}$ substitution mostly in the dravite–magnesio-foitite phase and (3) extensive Al–Mg disorder which even more enriches the *Y* site in Al and decreases the $^Y\!Mg$ content.

Dravite from Prosetín has blue–grey color which is typical especially of Li-bearing and rather less frequent in Mg-dominant tourmalines. Similar blue dravite was
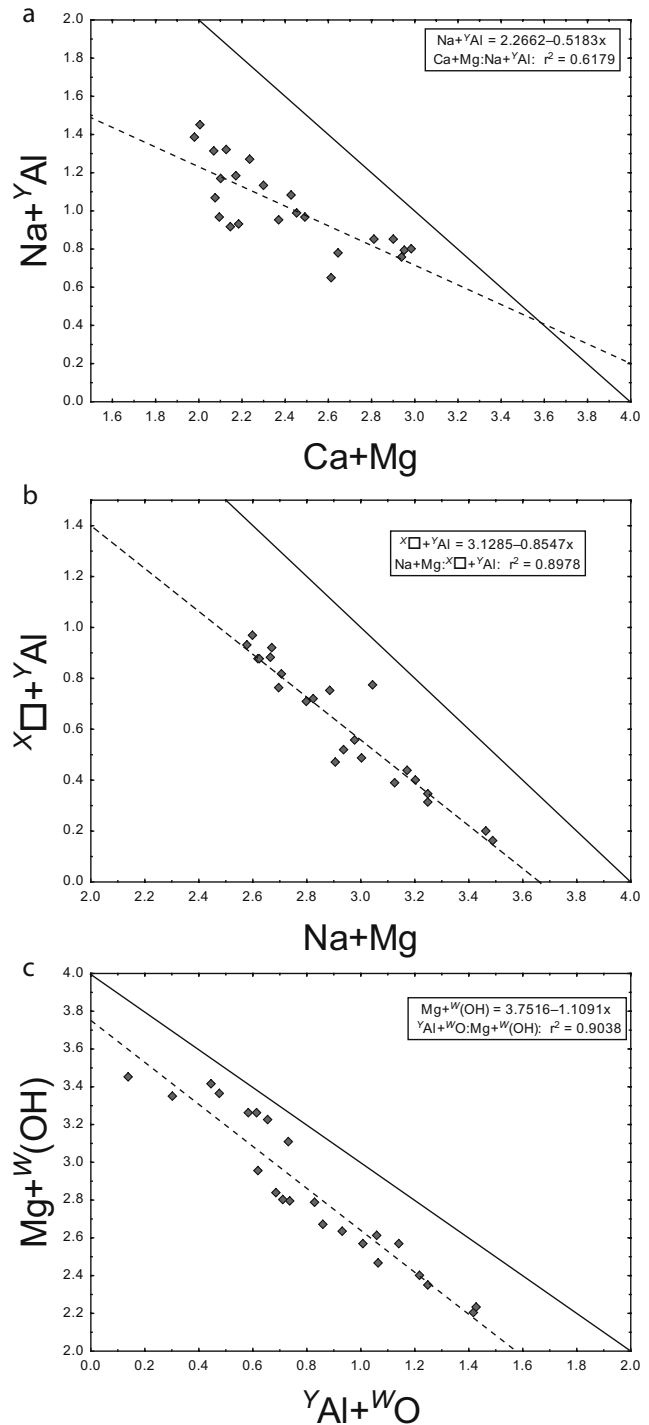
Fig. 5 Substitution diagrams of tourmaline from Prosetín: **a** – substitution CaMg(Na$^Y\!$Al)$_{-1}$; **b** – substitution NaMg($^X\!\square^Y\!$Al)$_{-1}$; **c** – substitution $^Y\!$Al$^W\!$O(Mg$^W\!$OH)$_{-1}$. Solid line represents ideal correlation, dashed line is the best linear fit to the data.

also described from several localities of Li-poor granitic pegmatites and marbles in the Moldanubicum, Czech Republic (Povondra 1981; Novák 1998) and also from Szkłary pegmatite, Poland (Pieczka 2007). It has been shown that the blue color in tourmaline is related to the

Ti = -48.5146 + 0.0437×Ca
Ca:Ti: r^2 = 0.7241

Sr = 35.2284 + 0.0265×Ca
Ca:Sr: r^2 = 0.7734
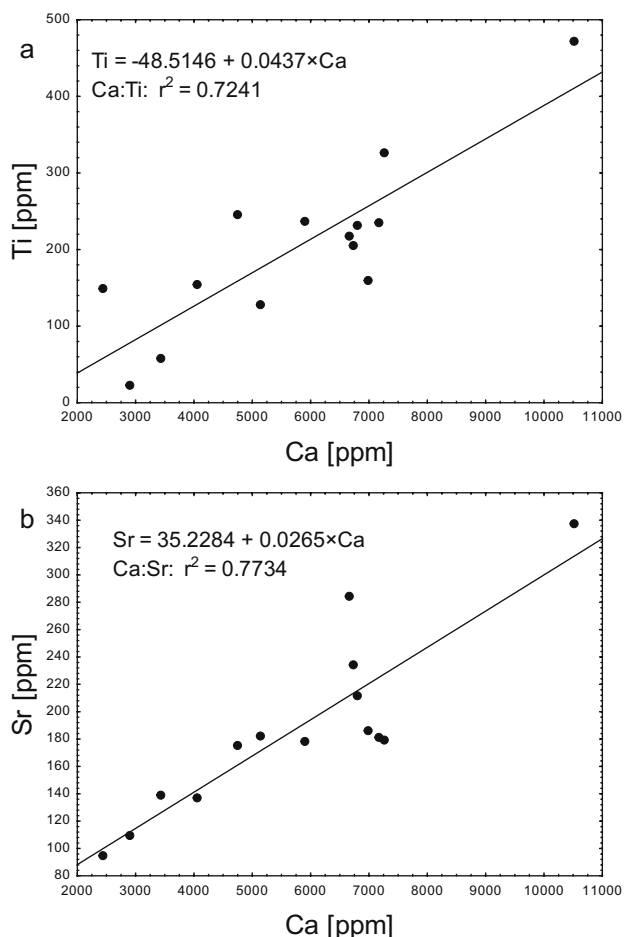
Fig. 6 Binary diagrams of trace elements in Prosetín tourmaline (LA-ICP-MS data in ppm): **a** – Ti vs. Ca; **b** – Sr vs. Ca. Solid line represents the best linear fit to the data.

spin-allowed crystal field transitions of Fe^{2+} in deformed octahedral sites while usual inter-valence charge transfer transitions (Fe^{2+}–Ti^{4+}, Fe^{2+}–Fe^{3+}) are responsible for brown and red–brown colors (e.g., Mattson and Rossman 1987; Cempírek et al. 2006; da Fonseca-Zang et al. 2008). High Fe^{3+} and Ti^{4+} contents cause dark (macroscopically black) color of Fe-rich tourmalines (e.g., Pieczka 2007; da Fonseca-Zang et al. 2008). All three tourmaline types from Prosetín are extremely Ti poor but contain significant amounts of Fe^{2+}. Hence their blue–grey color is most likely a result of Fe^{2+} crystal field transitions along with the presence of only limited amounts of other chromophores.

5.2 Origin of tourmaline and plagioclase–muscovite–scapolite rocks

The tourmaline composition, including trace elements, can be efficiently used to mark its genetic environment. The fibrous form of the Prosetín tourmaline and its low Ca content indicates fast non-equilibrium crystalliza-

tion from Na-rich fluid, along with low degree of *in situ* contamination. The zoning pattern with *X*-site vacant tourmaline core and dravitic rim resembles tourmalines grown in the prograde metamorphic environment (e.g., Henry and Dutrow 1996; Bačík et al. 2011b; Gieré et al. 2011). In contrast, tourmalines in granitic pegmatites usually display reverse zoning with rimward decrease in Ti and Mg and increase in Al and *X*-site vacancy, which indicate decreasing temperature and increasing degree of fractionation of the melt (e.g., Jolliff et al. 1987; Selway et al. 1999, 2000). Moreover, similar oxy-dravite to povondraite solid solution is typical of the metaevaporitic environment (Henry et al. 1999, 2008; Žáček et al. 2000; Bačík et al. 2008).

Contents of trace elements in tourmaline from Prosetín are relatively low, including the most abundant Ti, Sr and Ga (Tab. 4). Clearly, similar effective ionic radii of Ga^{3+} and Al^{3+} in octahedral and tetrahedral coordination (Shannon 1976) enable their mutual substitution in *Y*-, *Z*- and *T*-site positions of the tourmaline structure. Such a relationship between Al and Ga was observed also in tourmalines where Ga may attain tens to hundreds of ppm (e.g., Roda-Robles et al. 2004; Novák et al. 2011; Bačík et al. in print). Increased content of Sr can be related to the host-rock environment; Sr is one of the most abundant elements in seawater, *c.* 8 ppm (Faure 1977) which could support evaporitic origin of plagioclase–muscovite–scapolite rocks in Prosetín. The concentrations of other trace elements in the studied tourmalines, such as Mn, Zn, Sn and Li, are markedly lower compared to those reported from pegmatite tourmalines (e.g., Hellingwerf et al. 1994; Keller et al. 1999; Roda-Robles et al. 2004; Ertl et al. 2006; Novák et al. 2011; Bačík et al. in print).

The form of occurrence, major- and trace-element compositions of the Prosetín magnesian tourmaline imply rather non-magmatic (i.e., not aplitic or pegmatitic) origin. The new data support the idea of metaevaporitic source of the muscovite–plagioclase–scapolite rocks and formation of the magnesian tourmaline towards the end of the prograde metamorphic phase, as suggested by Opletal et al. (2007). Since the abundance of Cl- and B-rich minerals (scapolite and tourmaline) in some Moldanubian marbles and in associated metapelitic rocks points to their metaevaporitic origin (Kříbek et al. 1997; Houzar and Novák 2002), further detailed research of tourmaline crystal chemistry is desirable to improve our understanding of its behavior in metacarbonate systems.

References

Bačík P, Uher P, Sýkora M, Lipka J (2008) Low-Al tourmalines of the schorl–dravite–povondraite series in redeposited tourmalinites from the Western Carpathians, Slovakia. Canad Mineral 46: 1117–1129

Bačík P, Dianiška I, Števko M, Sečkár P (2011a) Brown finely acicular dravite from talc–magnesite deposit Gemerská Poloma (Gemeric Superunit, Slovakia). Bull mineral-petrolog Odd Nár Muz (Praha) 19: 164–167 (in Slovak)

Bačík P, Méres Š, Uher P (2011b) Vanadium-bearing tourmaline in metacherts from Chvojnica, Slovak Republic: crystal chemistry and multi-stage evolution. Canad Mineral 49: 195–206

Bačík P, Uher P, Ertl A, Jonsson E, Nysten P, Kanický V, Vaculovič T (in print) Zoned REE-enriched dravite from a granitic pegmatite in Forshammar, Bergslagen Province, Sweden: EMPA, XRD and LA-ICP-MS study. Canad Mineral 50.

Bloodaxe ES, Hughes JM, Dyar MD, Grew ES, Guidotti CV (1999) Linking structure and chemistry in the schorl–dravite series. Amer Miner 84: 922–928

Bosi F (2011) Stereochemical constraints in tourmaline: from a short-range to a long-range structure. Canad Mineral 49:17–27

Bosi F, Lucchesi S (2004) Crystal chemistry of the schorl–dravite series. Eur J Mineral 16: 335–344

Bosi F, Lucchesi S (2007) Crystal chemical relationships in the tourmaline group: structural constraints on chemical variability. Amer Miner 92: 1054–1063

Bosi F, Andreozzi GB, Federico M, Graziani G, Lucchesi S (2005) Crystal chemistry of the elbaite–schorl series. Amer Miner 90: 1784–1792

Burns PC, MacDonald DJ, Hawthorne FC (1994) The crystal chemistry of manganese-bearing elbaite. Canad Mineral 32: 31–41

Cempírek J, Novák M, Ertl A, Hughes JM, Rossman GR, Dyar MD (2006) Fe-bearing olenite with tetrahedrally coordinated Al from an abyssal pegmatite of the Bohemian Massif at Kutná Hora: structure, crystal chemistry, and optical spectra. Canad Mineral 44: 23–30

da Fonseca-Zang WA, Zang JW, Hofmeister W (2008) The Ti-influence on the tourmaline colour. J Brazil Chem Soc 19: 1186–1192

Ertl A, Hughes JM, Prowatke S, Ludwig T, Prasad PSR, Brandstätter F, Körner W, Schuster R, Pertlik F,

Marschall H (2006) Tetrahedrally coordinated boron in tourmalines from the liddicoatite–elbaite series from Madagascar: structure, chemistry, and infrared spectroscopic studies. Amer Miner 91: 1847–1856

Ertl A, Rossman GR, Hughes JM, Ma C, Brandstätter F (2008) V^{3+}-bearing, Mg-rich, strongly disordered olenite from a graphite deposit near Amstall, Lower Austria: a structural, chemical and spectroscopic investigation. Neu Jb Mineral, Abh 184: 243–253

Ertl A, Mali H, Schuster R, Körner W, Hughes JM, Brandstätter F, Tillmanns E (2010) Li-bearing, disordered Mg-rich tourmaline from a pegmatite–marble contact in the Austroalpine basement units (Styria, Austria). Mineral Petrol 99: 89–104

Faure G (1977) Principles of Isotope Geology. John Wiley & Sons, New York, pp 1–464

Finger F, Gerdes A, Janoušek V, René M, Riegler G (2007) Resolving the Variscan evolution of the Moldanubian sector of the Bohemian Massif: the significance of the Bavarian and the Moravo–Moldanubian tectonometamorphic phases. J Geosci 52: 9−28

Foit Jr FF (1989) Crystal chemistry of alkali-deficient schorl and tourmaline structural relationships. Amer Miner 74: 422–431

Gieré R, Rumble D, Günther D, Connolly J, Caddick MJ (2011) Correlation of growth and breakdown of major and accessory minerals in metapelites from Campolungo, Central Alps. J Petrol 52: 2293–2334

Grice JD, Ercit TS (1993) Ordering of Fe and Mg in tourmaline: the correct formula. Neu Jb Mineral, Abh 165: 245–266

Hawthorne FC (2002) Bond-valence constraints on the chemical composition of tourmaline. Canad Mineral 40: 789–797

Hawthorne FC, MacDonald DJ, Burns PC (1993) Reassignment of cation site occupancies in tourmaline: Al–Mg disorder in the crystal structure of dravite. Amer Miner 78: 265–270

Hawthorne FC, Selway JB, Kato A, Matsubara S, Shimizu M, Grice JD, Vajdak J (1999) Magnesiofoitite, □(Mg$_2$Al)Al$_6$(Si$_6$O$_{18}$)(BO$_3$)$_3$(OH)$_4$, a new alkali-deficient tourmaline. Canad Miner 37: 1439–1443

Hellingwerf RH, Gatedal K, Gallagher V, Baker JH (1994) Tourmaline in the central Swedish ore district. Miner Depos 29: 189–205

Henry DJ, Dutrow BL (1996) Metamorphic tourmaline and its petrologic applications. In: Grew ES, Anowitz LM (eds) Boron. Mineralogy, Petrology and Geochemistry. Mineralogical Society of America and Geochemical Society Reviews in Mineralogy and Geochemistry 33: 503–557

Henry DJ, Guidotti CV (1985) Tourmaline as a petrogenetic indicator mineral: an example from the staurolite-grade metapelites of NW Maine. Amer Miner 70: 1–15

Henry DJ, Kirkland BL, Kirkland DW (1999) Sector zoned tourmaline from the cap rock of a salt dome. Eur J Mineral 11: 263–280

Henry DJ, Sun H, Slack J, Dutrow BL (2008) Tourmaline in meta-evaporites and highly magnesian rocks: perspectives from Namibian tourmalinites. Eur J Mineral 20: 889–904

Houzar S, Leichmann J (2003) Application of cathodoluminescence to the study of metamorphic textures in marbles from the eastern part of the Bohemian Massif. Bull Geosci 78: 241−250

Houzar S, Novák M (2002) Marbles with carbonatite-like geochemical signature from variegated units of the Bohemian Massif, Czech Republic, and their geological significance. J Czech Geol Soc 47: 103−109

Houzar S, Němečková M, Novák M (2000) A report on research of tremolite marbles at Kuroslepy in west Moravia (Olešnice Group, Moravicum). Geol Výzk Mor Slez 1999: 120−122 (in Czech)

Hughes JM, Ertl A, Dyar MD, Grew ES, Shearer CK, Yates MG, Guidotti CV (2000) Tetrahedrally coordinated boron in a tourmaline: boron-rich olenite from Stoffhütte, Koralpe, Austria. Canad Miner 38: 861–869

Jolliff BL, Papike JJ, Laul JC (1987) Mineral recorders of pegmatite internal evolution: REE contents of tourmaline from the Bob Ingersoll pegmatite, South Dakota. Geochim Cosmochim Acta 51: 2225–2232

Kalvoda J, Bábek O, Fatka O, Leichmann J, Melichar R, Nehyba S, Špaček P (2008) Brunovistulian Terrane (Bohemian Massif, Central Europe) from late Proterozoic to late Paleozoic: a review. Int J Earth Sci (Geol Rundsch) 97: 497–518

Keller P, Roda Robles E, Pesquera Pérez A, Fontan F (1999) Chemistry, paragenesis and significance of tourmaline in pegmatites of the Southern Tin Belt, central Namibia. Chem Geol 158: 203–225

Křibek B, Hladíková J, Frýda J (1997) Scapolite and anhydrite-bearing rocks from the Moldanubian zone of the Bohemian Massif: Metamorphosed exhalites and evaporites. J Czech Geol Soc 42: 62

MacDonald DJ, Hawthorne FC, Grice JD (1993) Foitite, $\square[Fe^{2+}_2(Al,Fe^{3+})]Al_6Si_6O_{18}(BO_3)_3(OH)_4$, a new alkali-deficient tourmaline: description and crystal structure. Amer Miner 78: 1299–1303

Mattson SM, Rossman GR (1987) Identifying characteristics of charge transfer transitions in minerals. Phys Chem Miner 14: 94–99

Neubauer F, Handler R (2000) Variscan orogeny in the Eastern Alps and Bohemian Massif: how do these units correlate? Mitt Österr Geol Ges 92: 35−59

Novák M (1998) Blue dravite as an indicator of fluid composition during subsolidus replacement processes in Li-poor granitic pegmatites in the Moldanubicum, Czech Republic. J Czech Geol Soc 43: 24–30

Novák M, Škoda R, Filip J, Macek I, Vaculovič T (2011) Compositional trends in tourmaline from intragranitic NYF pegmatites of the Třebíč Pluton, Czech Republic: an electron microprobe, Mössbauer and LA–ICP-MS study. Canad Mineral 49: 359–380

Opletal V (2009) Metamorphic evolution of carbonate–evaporitic sedimentary complex in the Vranov–Olešnice Group of the Moravicum. Unpublished Thesis, Faculty of Natural Science, Masaryk University, Brno, pp 1−67 (in Czech)

Opletal V, Houzar S, Leichmann J (2007) Muscovite–plagioclase layers in dolomite marble near Prosetín (Olešnice Unit, Moravicum) concordant injections of aplite or metaevaporites? Acta Mus Moraviae, Sci Geol 92: 131–142 (in Czech)

Pieczka A (2007) Blue dravite from the Szkłary pegmatite (Lower Silesia, Poland). Mineralogia 38: 209–218

Pouchou JL, Pichoir F (1985) "PAP" (φρZ) procedure for improved quantitative microanalysis. In: Armstrong JT (ed) Microbeam Analysis. San Francisco Press, San Francisco, pp 104–106

Povondra P (1981) Crystal chemistry of tourmalines of the schorl–dravite series. Acta Univ Carol, Geol 3: 223–264

Povondra P, Novák M (1986) Tourmalines in metamorphosed carbonate rock from western Moravia, Czechoslovakia. Neu Jb Mineral, Mh 1986: 273–282

Roda-Robles E, Pesquera A, Gil PP, Torres-Ruiz J, Fontan F (2004) Tourmaline from the rare-element Pinilla pegmatite (Central Iberian Zone, Zamora, Spain): chemical variation and implications for pegmatitic evolution. Mineral Petrol 81: 249–263

Schulmann K, Ledru P, Autran A, Melka R, Lardeaux JM, Urban M, Lobkowicz M (1991) Evolution of nappes in the eastern margin of the Bohemian Massif: a kinematic interpretation. Geol Rundsch 80: 73−92

Schulmann K, Lexa O, Štípská P, Racek M, Tajčmanová L, Konopásek J, Edel JB, Peschler A, Lehmann J (2008) Vertical extrusion and horizontal channel flow of orogenic lower crust: key exhumation mechanism in large hot orogens? J Metamorph Geol 26: 273−297

Sekanina J (1965a) Minerals and their genetic relationships to rocks in area of geological map 1:50 000, part M 33-93-B (Bystřice nad Pernštejnem). Unpublished Manuscript, Department of Mineralogy and Petrology, Moravian Museum, Brno, pp 1−171 (in Czech)

Sekanina J (1965b) Vermiculit am Kontakt zwischen Aplit und Dolomit bei Prosetín (Nordteil der Schwarzawakuppel). Acta Univ Carol, Geol 2: 17–30

Selway JB, Novák M, Hawthorne FC, Černý P, Ottolini L, Kyser TK (1998) Rossmanite, $\square(LiAl_2)Al_6(Si_6O_{18})(BO_3)_3(OH)_4$, a new alkali-deficient tourmaline: description and crystal structure. Amer Miner 83: 896–900

Selway, JB, Novák M, Černý P, Hawthorne FC (1999) Compositional evolution of tourmaline in lepidolite-subtype pegmatites. Eur J Mineral 11: 569–584

SELWAY JB, ČERNÝ P, HAWTHORNE FC, NOVÁK M (2000) The Tanco pegmatite at Bernic Lake, Manitoba. Canad Mineral 38: 877–891

SHABYNIN LI (1973) Formation of Magnesian Skarns. Nauka, Moscow, pp 1–173 (in Russian)

SHANNON RD (1976) Revised effective ionic radii and systematic studies of interatomic distances in halides and chalcogenides. Acta Cryst A32: 751–767

ULRICH S, SCHULMANN K, CASEY M (2002) Microstructural evolution and rheological behaviour of marbles deformed at different crustal levels. J Struct Geol 24: 979−995

ŽÁČEK V, FRÝDA J, PETROV A, HYRŠL J (2000) Tourmalines of the povondraite–(oxy)dravite series from the cap rock of meta-evaporite in Alto Chapare, Cochabamba, Bolivia. J Czech Geol Soc 45: 3–12